The Roman eXtreme Deep Field (RXDF)

Haojing Yan[1], Anton M. Koekemoer[2], Yue Shen[3], Bangzheng Sun[1], Norman A. Grogin[2], Zihao Wu[4], Christian Kragh Jespersen[5], Rachel Somerville[6], Kyoung-Soo Lee[7], Dale D. Kocevski[8], Adam J. Burgasser[9], Pedro H. Bernardinelli[10], Yicheng Guo[1], Charles Steinhardt[1], Xiaohui Fan[11], Duncan Farrah[12], Gisella De Rosa[2], Feige Wang[13], Jinyi Yang[13], Lifan Wang[14], Fengwu Sun[4], Christopher N. A. Willmer[15], John David Silverman[16], Steven L. Finkelstein[17], Seth H. Cohen[18], Rolf A. Jansen[18], Rogier A. Windhorst[18], Brent M. Smith[18], Stefano Casertano[2], Anthony H. Gonzalez[19], Michael A. Strauss[5], Ray A. Lucas[2], Katherine E. Whitaker[20], Mingyang Zhuang[3], Rodrigo Angulo[21], Chloe Aurin[22], Micaela Bagley[17], Franz E. Bauer[23], Jessica M. Berkheimer[18], Rachel Bezanson[24], Alejandro S. Borlaff[25], Rebecca A. A. Bowler[26], Larry D. Bradley[2], W. N. Brandt[27], Denis Burgarella[22], Timothy Carleton[18], Delondrae D. Carter[18], Caitlin M. Casey[28], Christopher J. Conselice[26], Kyle W. Cook[29], Jeff Cooke[30], David A. Coulter[2], Tyler Desjardins[2], Tim Dewachter[22], Nicole E. Drakos[31], Simon P. Driver[32], Qiao Duan[33], Eiichi Egami[34], Andreas Faisst[35], Travis C. Fischer[2], Adriano Fontana[36], Ori Fox[2], Brenda Frye[37], Yoshinobu Fudamoto[38], Eric Gawiser[39], Mauro Giavalisco[20], Yuichi Harikane[40], Thomas Harvey[26], Nimish P. Hathi[41], Benne W. Holwerda[29], Taylor Hutchison[42], Olivier Ilbert[22], Akio K. Inoue[43], Lucy R. Ivey[33], Kartheik Iyer[6], Mathilde Jauzac[44], Ignas Juodžbalis[33], Jeyhan S. Kartaltepe[45], Daichi Kashino[46], Susan Kassin[2], Patrick Kelly[47], Kotaro Kohno[48], Stephanie LaMassa[2], Erini Lambrides[42], Rebecca Larson[2], Junyao Li[3], Zhiyuan Ma[20], Sangeeta Malhotra[42], Elizabeth McGrath[8], Peter Melchior[5], Marcio Mélendez[2], Hironao Miyatake[49], Bahram Mobasher[50], Mireia Montes[51], Thomas Moore[2], Takahiro Morishita[52], Takashi Moriya[46], Leonidas Moustakas[53], Rohan Naidu[54], Rosalia O'Brien[42], Pascal A. Oesch[55], Masafusa Onoue[56], Rafael Ortiz III[18], Masami Ouchi[57], Robert G. Pascalau[33], Molly Peeples[2], Andreea O. Petric[2], Sara Petty[58], Justin Pierel[2], Marc Rafelski[2], Enikő Regős[59], Armin Rest[2], Mitchell Revalski[2], James Rhoads[42], Pierluigi Rinaldi[2], Aaron Robotham[60], Kate Rowlands[2], Pablo M. Sánchez-Alarcón[25], Paola Santini[36], Alice E. Shapley[61], Raymond C. Simons[62], Swara Ravindranath[42], Takahiro Sumi[63], Takumi S. Tanaka[16], Masayuki Tanaka[46], Scott Tompkins[60], Christina C. Williams[64], Edward J. Wollack[42], John F. Wu[2] and L. Y. Aaron Yung[2]

[1] *Department of Physics and Astronomy, University of Missouri, Columbia, MO 65211, USA*

[2] *Space Telescope Science Institute, Baltimore, MD 21218, USA*

[3] *Department of Astronomy, University of Illinois Urbana-Champaign, Urbana, IL 61801, USA*

[4] *Center for Astrophysics | Harvard & Smithsonian, Cambridge, MA 02138, USA*

[5] *Department of Astrophysical Sciences, Princeton University, Princeton, NJ 08544, USA*

[6] *Center for Computational Astrophysics, Flatiron Institute, New York, NY 10010, USA*

[7] *Department of Physics and Astronomy, Purdue University, West Lafayette, IN 47906, USA*

[8] *Department of Physics and Astronomy, Colby College, Waterville, ME 04901, USA*

yanha@missouri.edu

koekemoer@stsci.edu

shenyue@illinois.edu

[9]*Department of Astronomy and Astrophysics, UC San Diego, La Jolla, CA, USA*
[10]*Instute for Astronomy, Geophysics and Atmospheric Sciences, University of São Paulo, SP, 05508-090, Brazil*
[11]*Department of Astronomy & Steward Observatory, University of Arizona, Tucson, AZ 85721, USA*
[12]*Department of Physics and Astronomy, University of Hawai'i at Mānoa, Honolulu, HI 96822, USA*
[13]*Department of Astronomy, University of Michigan, Ann Arbor, MI 48109, USA*
[14]*George P. and Cynthia Woods Mitchell Institute for Fundamental Physics & Astronomy, Department of Physics and Astronomy, Texas A. & M. University, College Station, TX 77843, USA*
[15]*Steward Observatory, University of Arizona, Tucson, AZ, 85721, USA*
[16]*Kavli Institute for the Physics and Mathematics of the Universe (WPI), Tokyo Institutes for Advanced Study, University of Tokyo, Chiba 277-8583, Japan*
[17]*Department of Astronomy, The University of Texas at Austin, Austin, TX, USA*
[18]*School of Earth & Space Exploration, Arizona State University, Tempe, AZ 85287-1404, USA*
[19]*Department of Astronomy, University of Florida, Gainesville, FL 32611, USA*
[20]*Department of Astronomy, University of Massachusetts, Amherst, MA 01003, USA*
[21]*Johns Hopkins University, William H. Miller III Department of Physics and Astronomy, Baltimore, MD 21218, USA*
[22]*Aix Marseille Université, CNRS, CNES, LAM, Marseille, France*
[23]*Institute of Advanced Studies, University of Tarapacá, P.O. Box 7D, Arica 1010000, Chile*
[24]*Department of Physics and Astronomy and PITT PACC, University of Pittsburgh, Pittsburgh, PA 15260, USA*
[25]*NASA Ames Research Center, Moffett Field, CA 94035, USA*
[26]*Jodrell Bank Centre for Astrophysics, University of Manchester, Manchester, M13 9PL, UK*
[27]*Department of Astronomy and Astrophysics, The Pennsylvania State University, PA 16802, USA*
[28]*Department of Physics, University of California, Santa Barbara, Santa Barbara, CA 93106, USA*
[29]*Department of Physics and Astronomy, University of Louisville, Louisville, KY 40292 USA*
[30]*Centre for Astrophysics and Supercomputing & ARC Centre of Excellence for Gravitational Wave Discovery (OzGrav), Swinburne University of Technology, Hawthorn, VIC 3122, Australia*
[31]*Department of Physics and Astronomy, University of Hawai'i, Hilo, HI 96720, USA*
[32]*International Centre for Radio Astronomy Research (ICRAR) and the International Space Centre (ISC), The University of Western Australia, M468, Crawley, WA 6009, Australia*
[33]*Kavli Institute for Cosmology, University of Cambridge, Cambridge CB3 0HA, UK*
[34]*Steward Observatory, University of Arizona, Tucson, AZ 85721, USA*
[35]*IPAC, California Institute of Technology, Pasadena, CA 91125, USA*
[36]*INAF - Osservatorio Astronomico di Roma, via Frascati 33, 00078 Monte Porzio Catone (Roma), Italy*
[37]*Department of Astronomy & Steward Observatory, University of Arizona, Tucson, AZ, 85721, USA*
[38]*Center for Frontier Science, Chiba University, Chiba 263-8522, Japan*
[39]*Department of Physics and Astronomy, Rutgers, the State University of New Jersey, Piscataway, NJ 08854, USA*
[40]*Institute for Cosmic Ray Research, The University of Tokyo, Kashiwa, Chiba 277-8582, Japan*
[41]*United States Patent and Trademark Office, Alexandria, VA 22314, USA*
[42]*Astrophysics Science Division, NASA, Goddard Space Flight Center, Greenbelt, MD 20771, USA*
[43]*Department of Physics, School of Advanced Science and Engineering, Waseda University, Tokyo 169-8555, Japan*
[44]*Centre for Extragalactic Astronomy, Durham University, Durham DH1 3LE, UK*
[45]*Laboratory for Multiwavelength Astrophysics, School of Physics and Astronomy, Rochester Institute of Technology, Rochester, NY 14623, USA*
[46]*National Astronomical Observatory of Japan, Tokyo 181-8588, Japan*
[47]*School of Physics and Astronomy, University of Minnesota, Minneapolis, MN 55455, USA*
[48]*Institute of Astronomy, The University of Tokyo, Mitaka, Tokyo 181-0015, Japan*

[49]Kobayashi-Maskawa Institute for the Origin of Particles and the Universe, Nagoya University, Nagoya 464-8602, Japan
[50]Department of Physics & Astronomy, University of California, Riverside, Riverside, CA 92521, USA
[51]Institute of Space Sciences (ICE, CSIC), Campus UAB, Carrer de Can Magrans, s/n, 08193 Barcelona, Spain
[52]Astronomical Institute, Tohoku University, 6-3, Aramaki, Aoba, Sendai, Miyagi 980-8578, Japan
[53]Jet Propulsion Laboratory, California Institute of Technology, Pasadena, CA 91109, USA
[54]MIT Kavli Institute for Astrophysics and Space Research, Cambridge, MA 02139, USA
[55]Department of Astronomy, University of Geneva, Chemin Pegasi 51, 1290 Versoix, Switzerland
[56]Waseda Institute for Advanced Study (WIAS), Waseda University, Tokyo 169-0051, Japan
[57]Institute for Cosmic Ray Research, The University of Tokyo, Chiba 277-8582, Japan
[58]NorthWest Research Associates, Boulder, CO 80301, USA
[59]Konkoly Observatory HUN-REN CSFK, Konkoly-Thege M. ut 15-17, Budapest, 1121, Hungary
[60]International Centre for Radio Astronomy Research (ICRAR) and the International Space Centre (ISC), The University of Western Australia, Crawley, WA 6009, Australia
[61]Department of Physics & Astronomy, University of California, Los Angeles, Los Angeles, CA 90095, USA
[62]Engineering & Physics, Providence College, Providence, RI 02918, USA
[63]Department of Earth and Space Science, The University of Osaka, Toyonaka, Osaka 560-0043, Japan
[64]NSF National Optical-Infrared Astronomy Research Laboratory, Tucson, AZ 85719, USA

Abstract

The Roman eXtreme Deep Field (RXDF) program is one of the five General Astrophysics Survey (GAS) programs approved for observing time with the Nancy Grace Roman Space Telescope in Cycles 1 and 2. It has been allocated 386.41 hours to carry out an imaging survey to AB = 30 mag (5σ) over $\sim$140$\times$ larger area than the Hubble eXtreme Deep Field (HXDF) full-depth area (ACS+WFC3/IR). The RXDF will cover the full Roman wavelength range with 7 bands, reaching AB = 30 mag in $RZYJH$, 29 mag in F, and 28 mag in K, over a full-depth area of 678.75 arcmin^2 embedded in a total area of 1,243 arcmin^2, and far exceeding the depths of the Roman Core Community Surveys (CCS). The RXDF is within the Euclid Ultra Deep Field (EUDF) near the North Ecliptic Pole (NEP), a strategic long-term field for generational space facilities, with a wealth of multi-wavelength data including extensive coverage from the James Webb Space Telescope (JWST) NEXUS Treasury program. The observations will cover 3 epochs at a 1-year cadence, each epoch divided into 3 sub-epochs $\sim$10 days apart, enabling time-domain studies on time baselines from $\sim$10 days to over $\sim$2 years. The RXDF is uniquely positioned to address critical questions in reionization, large scale structure (LSS), growth of supermassive black holes (SMBHs), little red dots (LRDs), and high-z supernovae (SNe); the volumes probed by HST+JWST are too small at these extreme depths, and even the deepest CCS tiers are too shallow. In addition to our key objectives, a wealth of additional science will be enabled by engaging the community with our rapidly released datasets, revolutionizing a wide range of science for a lasting legacy. This short document, which is converted from the approved RXDF proposal, aims to provide the community with a summary of the program.

1. SYNOPSIS

JWST has made many new discoveries at the faintest magnitudes across all redshifts, but addressing the questions raised by these discoveries will require studies to AB $\sim$30 mag over a much larger area than JWST's reach. The Roman eXtreme Deep Field (RXDF; Roman PID 2001, PI H. Yan, co-PIs A. Koekemoer and Y. Shen) will answer this call by carrying out 7-band, 0.5–2.3 μm imaging in one WFI pointing in the North Ecliptic Pole (NEP) region within the Euclid Ultra-Deep Field (EUDF), part of which is being observed by the North ecliptic pole EXtragalactic Unified Survey (NEXUS; Shen et al. 2024), a JWST multicycle (Cycle 3–5) Treasury program (JWST PID 5105, PI Y. Shen). RXDF will reach 5σ limits [1] of AB = 30 mag in $RZYJH$, 29 mag in F, and 28 mag in K, which far exceed the "deep/ultra-deep" parts of the Core Community Surveys (CCS; see Table 1). To enable time-domain science, RXDF will be split into three main epochs with a $\sim$1-yr cadence (the 3$^{\rm rd}$ epoch could be in Year 3 of mission operations, depending on scheduling), with each epoch further divided into three sub-epochs $\sim$10 days apart. RXDF will enable unique studies of galaxies from $z \approx 14$ to $z < 2$, probe AGN to unprecedented low luminosities, and hunt for faint transients out to $z \gtrsim 5$.

	F062 (R)	F087 (Z)	F106 (Y)	F129 (J)	F158 (H)	F184 (F)	F213 (K)
RXDF	30.6 hrs	53.5 hrs	55.4 hrs	65.4 hrs	73.2 hrs	36.5 hrs	60.4 hrs
5σ, $r = 0.2''$	30.0 mag	30.0 mag	30.0 mag	30.0 mag	30.0 mag	29.0 mag	28.0 mag
HLTDS stack	—	7.7 hrs	5.9 hrs	6.1 hrs	8.4 hrs	37.2 hrs	—
5σ, $r = 0.2''$	—	28.75 mag	28.68 mag	28.63 mag	28.77 mag	28.96 mag	—
HLWAS D+UD	—	1.23 hrs	3.68 hrs	3.68 hrs	3.68 hrs	1.23 hrs	1.23 hrs
5σ, $r = 0.2''$	—	27.7 mag	28.2 mag	28.2 mag	28.1 mag	27.0 mag	25.9 mag

Table 1. Comparison of integration times and depths in RXDF and the two Community Core Surveys, the HLTDS 2-year stack and the HLWAS "Deep" (D) and "Ultra-deep" (UD).

2. RATIONALE

The iconic Hubble Ultra Deep Field (HUDF; Beckwith et al. 2006), subsequently observed with more programs and reprocessed as the Hubble eXtreme Deep Field (HXDF; Oesch et al. 2010; Ellis et al. 2013; Illingworth et al. 2013; Teplitz et al. 2013), invested $\sim$520 hours to reach AB $\sim 29.7-30.0$ mag in most filters across $\sim$0.4$-$1.6 μm with ACS and WFC3/IR over 4.7 arcmin^2. The deepest JWST imaging has likewise invested $\sim$360 hours to reach AB $\sim 30.1-30.9$ mag over $\sim$9 arcmin^2 (Eisenstein et al. 2025, 2026). But significantly extending these small areas at such depths is infeasible with these telescopes. With Roman's Wide Field Instrument (WFI), RXDF will reach AB $\sim$ 30 mag over $\sim$144$\times$ larger area than the full-depth ACS+WFC3/IR HXDF, revolutionizing studies of the deep universe.

- **Why 7 Bands?** The new science goals demand full Roman wavelength coverage with sufficient sampling for SED analysis (e.g., Bagley et al. 2025). In particular, R (F062) is outside the range of JWST, while Euclid lacks K (F213). Both are critical in making RXDF unique among deep surveys.
- **Why Now?** Roman's first two cycles will be within Euclid's last three years and in the middle of its last $\sim$40 cadenced visits in the EUDF. Executing RXDF early will ensure direct synergy with

[1] Throughout this document, the depths are quoted as 5σ limiting magnitudes within an $r = 0\farcs2$ circular aperture.

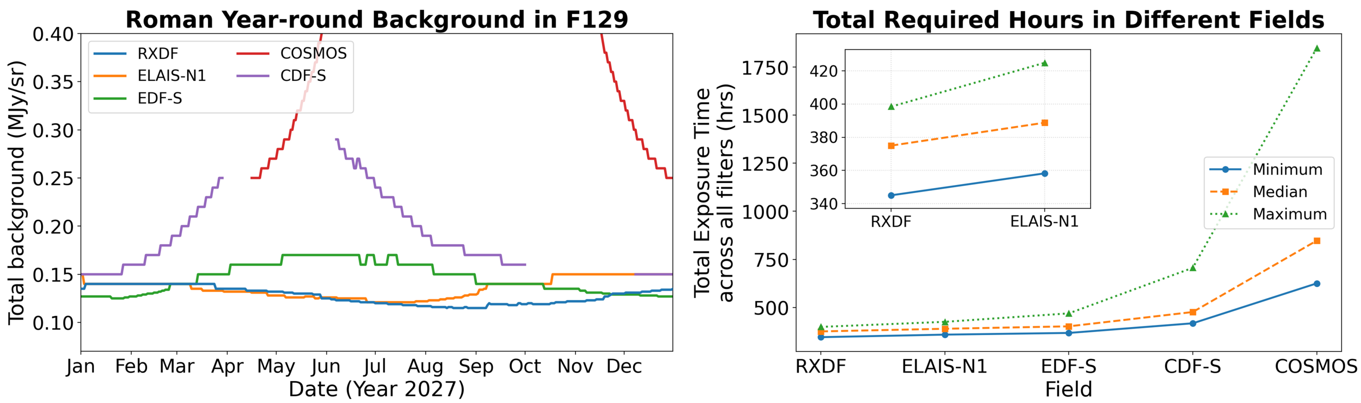

Figure 1. (**left**) Total backgrounds in various extragalactic fields in their respective observing windows throughout a year, using F129 as example. (**right**) Total number of hours needed in these fields to reach our desired depths, which are affected by the changing zodiacal background in a year. For each field, the minimum (blue), maximum (green) and median (orange) number of hours are shown. The inset shows the comparison between RXDF and ELAIS-N1.

Euclid time-domain science. Furthermore, some of our discoveries will require prompt JWST follow-up at >2 μm; an early synergy with JWST will maximize the science returns from both observatories.

• **Why choose this NEP field?** Besides the synergy with the EUDF and a myriad of deep data from radio to X-rays, our field has the lowest zodiacal background year-round compared to other fields and is thus the most suitable for creating an ultra-deep field with high efficiency (Figure 1). The NEP region is within the continuous viewing zone (CVZ) of Roman, which makes the RXDF highly flexible in terms of scheduling. Furthermore, the field is also within JWST's CVZ, and our high-value targets (especially transients) can be promptly observed by JWST at any time. It already has JWST NIRCam imaging (F090W, F115W, F150W, F200W, F356W, F444W) covering ∼400 arcmin^2 to 5σ limits of AB = (26.9, 26.8, 26.8, 28.0, 27.6, 27.8) mag from the JWST NEXUS program. The NEP field has critical long-term strategic value for extragalactic science in the era of space survey facilities. Synergies with other facilities are further discussed below.

• **Can it be done in a Roman CCS field to save time?** No. The most favorable alternative would be ELAIS-N1, which was chosen by the High Latitude Time Domain Survey (HLTDS) as its northern field for its slightly lower Galactic reddening (E(B-V)=0.01 mag) than NEP, and this is important for the main science of the HLTDS on low-z type Ia supernovae (SNe Ia). However, ELAIS-N1 still has significantly higher background for ∼5 months of the year, and avoiding this would put substantial pressure on observatory scheduling. Moreover, even if we put the RXDF on top of the HLTDS 2-yr stack, it would not become a "time-saver" for two reasons. Firstly, the HLTDS stack would only be equivalent to a small fraction of the time that RXDF will need. Due to the short exposures used, the HLTDS is noticeably impacted by readout noise in most filters except in F184. The full-depth exposure times listed in Table 1 would be equivalent to $(Z, Y, J, H, F) = (5.4, 4.9, 5.2, 7.6, 33.9)$ hrs in our adopted long-integration mode, and the possible time saving would not offset the cost due to its higher background. Secondly, more subtle but as important, the HLTDS observing strategy will not fully cover the wide detector gaps and will have severely non-uniform integrations across the stack (see Figure 2). Its full-depth area would amount to only 21.1 arcmin^2 and would

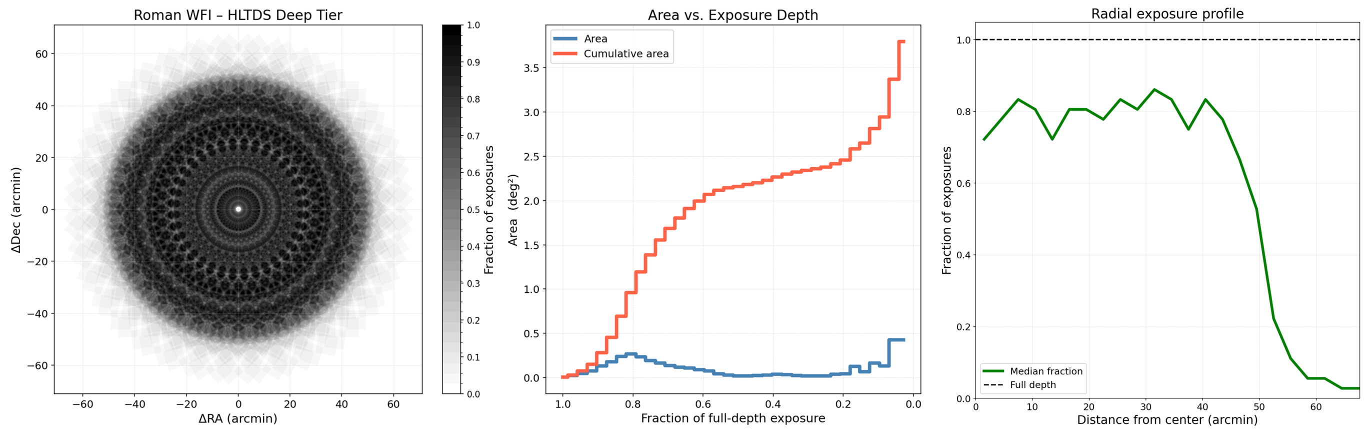

Figure 2. (*left*) Exposure map of the 2-yr HLTDS stack, demonstrating its severe non-uniformity. The scale bar indicates the fractional integration with respect to the full-depth exposure. (*middle*) Differential (blue) and cumulative (red) areas as functions of fractional integration time. (*right*) Radial profile of the exposure map, calculated in annuli of 3 arcmin width.

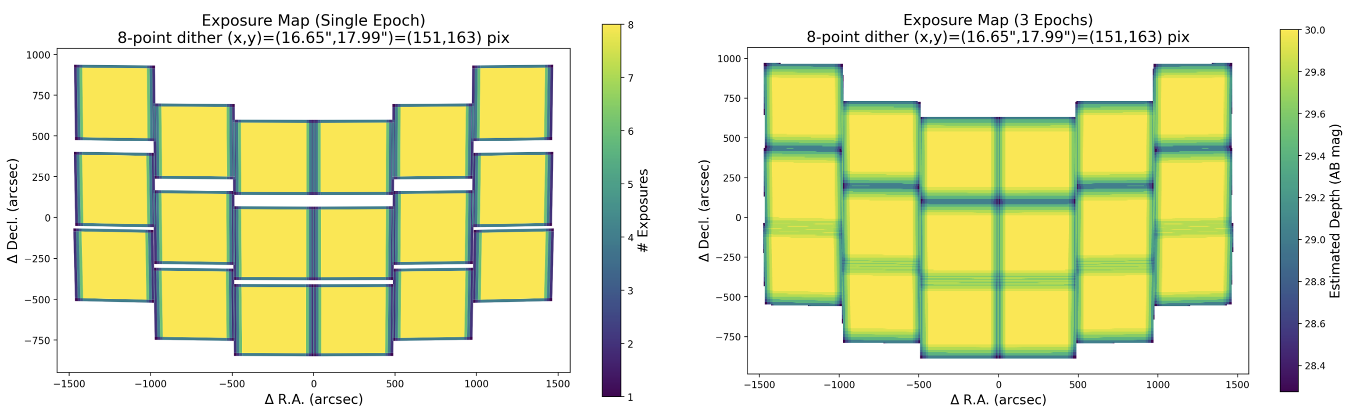

Figure 3. (**left**) RXDF exposure map in a single sub-epoch (there being three sub-epochs in each main epoch), where the gaps between detectors are partially filled by our customized 8-point dithering pattern. The color bar scale indicates the number of overlapped exposures. (**right**) Exposure map of the 3-yr stack made out of three main epochs (nine sub-epochs). The gaps are filled by moving the field center slightly in between the sub-epochs. The color bar scale indicates the 5σ depth in AB mag. The full-depth area amounts to 678.75 arcmin^2. The total, contiguous coverage is 1,243 arcmin^2.

be scattered over the field. For a representative WFI pointing at its field center, the typical HLTDS coverage would only have ~80% of the full depth, which further negates any possible time saving.

3. OBSERVATIONAL DESIGN

We aim to maximize depth over the full WFI footprint and will split the observations into 3 main epochs separated by ~1 yr. As the telescope's orientation rotates on a yearly basis, such a yearly cadence will ensure the same WFI FoV being repeated 3 times to maximize the overlapping (full-depth) area. Each main epoch is further divided into 3 sub-epochs separated by ~10−12 days, with position angle adjustments (allowed within ±15° at Roman) to maintain the same footprint. As

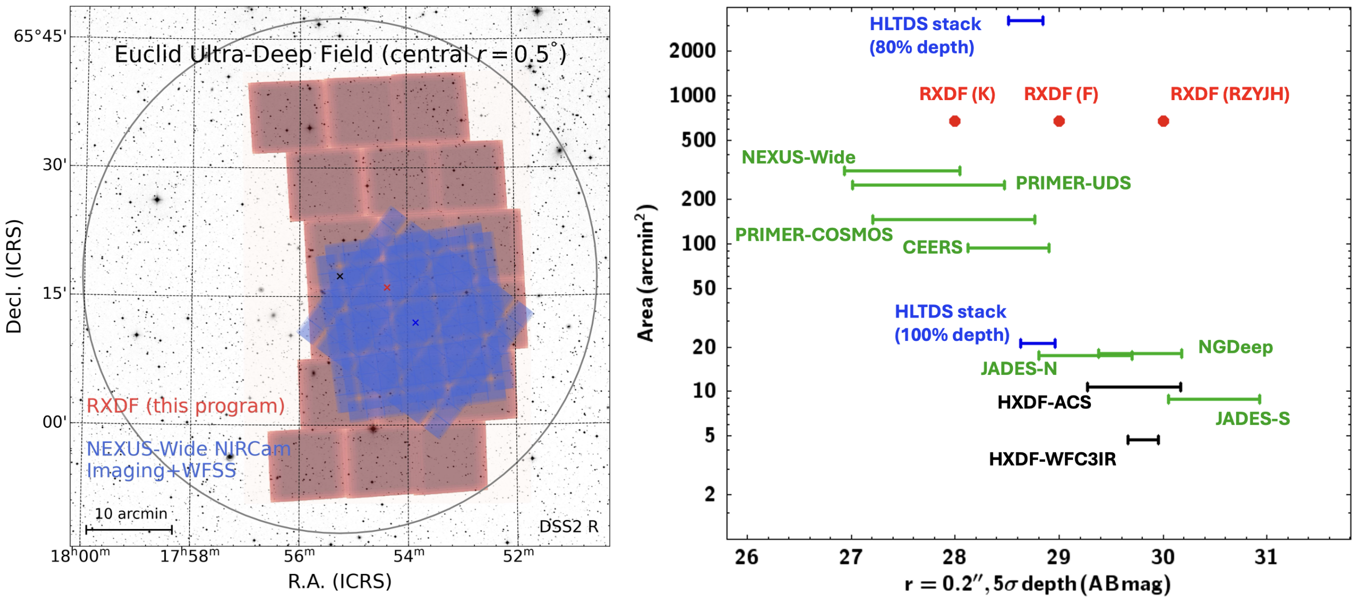

Figure 4. (**Left**) Overlay of RXDF on the center of EUDF (black circle) and its overlap with the JWST-NEXUS field (blue), at a representative orient. Regardless of the exact execution date, the RXDF footprint placement can always be chosen to be within the EUDF and to cover the JWST-NEXUS field. RXDF will reach $\sim$2.5 mag deeper than JWST-NEXUS over 0.8–1.7 μm and extend bluer to 0.5 μm. (**Right**) Depth and coverage of RXDF (red circles) as compared to HXDF (black), various JWST surveys to date (green) and Roman's HLTDS (blue). The depths of these other surveys are indicated by horizontal bars to reflect the different depths achieved in different bands involved.

the exposure maps in Figure 3 show, we will use a customized dithering pattern to cover the gaps between detectors so that they are all filled in the 3-yr stack while maximizing the full-depth area.

As demonstrated by numerous studies, proper SED analysis relies on a sufficient number of pass-bands covering the full range from optical to near-IR wavelengths (e.g., Illingworth et al. 2013; Bagley et al. 2025). We stress that neither R or K can be omitted: R will be critical for the studies not only at mid-z but also at high-z (Bagley et al. 2025), while K, even by just providing upper limits, will be crucial in distinguishing SEDs of AGNs and normal galaxies.

To minimize the impact of read-out noise, we will use >600 sec integration time. We adopt the 5-σ depth measured within an $r = 0\farcs2$ aperture for point sources, which is the Roman ETC's default for depth calculation. For each day within a cycle, we calculate the exposure times needed to reach the desired depths, and the median values are listed in Table 1. The total on-source time is 375 hrs; after taking the overhead into account (as calculated by the APT), the total charged time is 386.41 hrs, which is what our program has been approved for.

The RXDF footprint within the EUDF is demonstrated in the left panel of Figure 4, at a representative orientation. The right panel of this figure compares the RXDF depth and coverage to those of the HXDF, various JWST surveys to date and Roman's HLTDS.

4. KEY SCIENCE GOALS

RXDF will create a full-depth area of 678.75 arcmin^2, which is embedded in a contiguous coverage of 1,243 arcmin^2. The unprecedented combination of depth and area will minimize the impact of

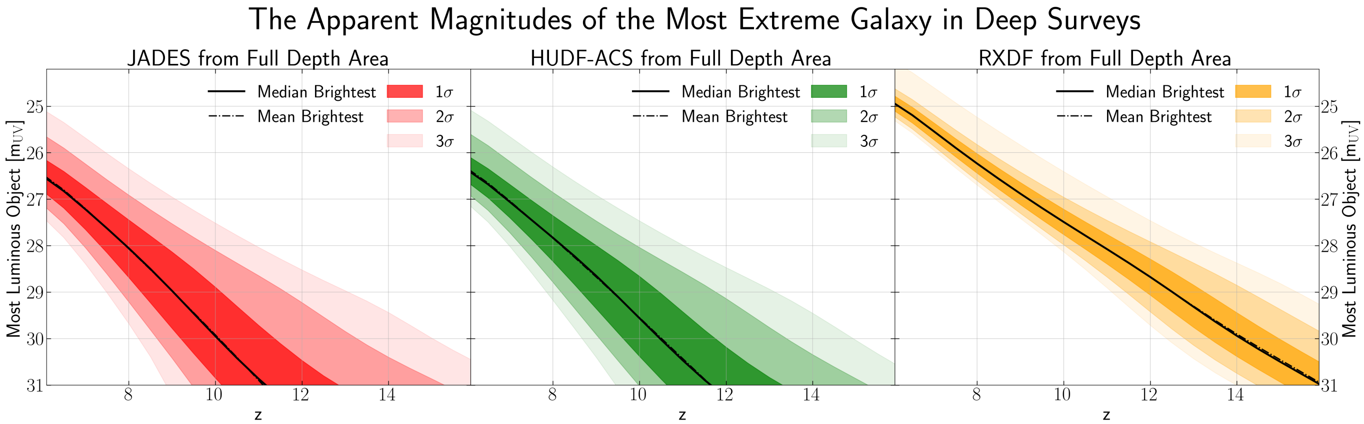

Figure 5. Impact of cosmic variance on characterizing rare objects due to the size of survey area, using the brightest galaxies at high-z as example. The probability contours of the brightest galaxy that could be found in areas of JADES, HUDF and RXDF (calculated following Jespersen et al. 2025) are shown from left to right. RXDF's large area increases the chance of finding such objects and greatly reduces the impact of cosmic variance when calculating their true number density.

cosmic variance for many studies. Figure 5 demonstrates this using the brightest galaxies at high-z as examples. We lay out below the unique science questions that only RXDF can properly address.

4.1. *Galaxies*

JWST has pushed the redshift frontier of galaxies to $z = 14.44$ (Naidu et al. 2026) and is likely to soon break the record again. These discoveries have raised numerous crucial questions at $z \lesssim 14$, and we highlight below a few key topics that can only be properly addressed by RXDF.

4.1.1. *Cosmic dawn*

Candidate galaxies can be selected as dropouts in successive bands from Z to F, reaching 30, 29 and 28 mag for those at $z \lesssim 10$, $z \approx 12$ and $z \approx 14$, respectively, which correspond to $M_{\rm UV} = -16.8$, -17.1, -17.5, -18.8, and -20.0 mag at $z \approx 6.2$, 7.7, 9.6, 12.0, and 14.1, respectively (Figure 2). By conservative estimates and after considering incompleteness, our sample will contain $\sim 10^4$, $\sim 5 \times 10^3$, $\sim 10^3$, ~ 100 and ~ 20 galaxies in these redshift ranges.

(1) *Galaxy luminosity function (LF):* Accurate measurements of galaxy LFs at $z \gtrsim 6$ have profound impact on our knowledge of early galaxy formation and reionization. RXDF's results will be decisive at both the bright and faint ends for the $z \lesssim 11$ LFs. At $z \gtrsim 12$, current LFs are highly uncertain due to small number statistics, but RXDF will impose the strongest constraints.

(2) *Constraining modes of star formation and host halo masses with clustering:* One of JWST's biggest surprises was the discovery of many more bright galaxies at $z > 10$ than expected. The two leading explanations are a higher overall star formation efficiency or more bursty star formation at earlier times (Somerville et al. 2025). These mechanisms have degenerate effects on the UVLF but make very different predictions for the host halo masses, M_h, that galaxies of a given luminosity occupy. Because halo clustering is a strong function of mass, the simultaneous measurements of LF and galaxy clustering can not only constrain the M_h-$L_{\rm UV}$ relationship but also the timescale of SF burstiness (Lee et al. 2009; Endsley et al. 2020; Muñoz et al. 2023; Sun et al. 2025).

As RXDF spans a large and contiguous area with largely uniform depth, we can measure the angular correlation function (ACF; e.g., Landy & Szalay 1993) or counts-in-cells (field to field variance) across

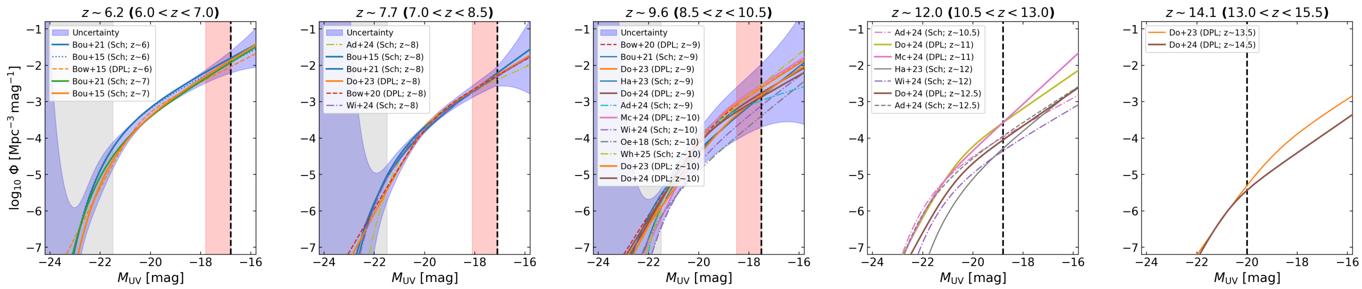

Figure 6. Current estimates of UVLF at $6 \lesssim z \lesssim 14$, taken from Adams et al. (2024); Bouwens et al. (2015, 2021); Bowler et al. (2015, 2020); Donnan et al. (2023, 2024); Harikane et al. (2023a); McLeod et al. (2024); Oesch et al. (2018); Whitler et al. (2025); Willott et al. (2024). The RXDF limits are shown by the vertical dashed lines. The blue area in the first three panels indicates the 1σ uncertainty, while the grey and red shaded regions indicate the regimes where RXDF will provide decisive results. The LFs at $z \gtrsim 12$ are highly uncertain, and our results will impose the strongest constraints. All this is owing to the minimal cosmic variance in RXDF as compared to any other (including JWST) surveys.

a broad range of luminosities, from bright objects inaccessible to pencil-beam surveys like JADES to faint objects missed by shallow wide-field surveys like COSMOS-Web (as discussed for example by Paquereau et al. 2025; Dalmasso et al. 2026). These measurements will yield accurate constraints on the relationship between UV luminosity and host halo mass, discriminate between different theoretical scenarios to explain the "excess" bright galaxies.

(3) *Early large scale structures (LSS):* The emergence of LSS at early epochs provides a critical constraint on the hierarchical formation theory. While JWST has revealed a few structures detected as galaxy overdensities as early as $z \approx 10.5$ (Tacchella et al. 2023; Scholtz et al. 2024; Wu et al. 2026), the abundance of such massive structures and how they develop over cosmic time remain unconstrained. Properly addressing this question requires a deep survey limit sufficient to detect low-luminosity members over a wide, contiguous area minimizing cosmic variance (Figure 7, left). RXDF will, for the first time, offer a unique opportunity to conduct a systematic LSS study over $6 \lesssim z \lesssim 14$.

4.1.2. *Cosmic noon to afternoon*

The epoch of $z \approx 2$–3 (cosmic noon) marks the peak of cosmic SFR density. After this peak, prevalent quenching leads to a rapid buildup of quiescent populations, especially in the low-mass regime (Muzzin et al. 2013). RXDF will detect dwarf galaxies down to $M_* \sim 10^{7.0}, 10^{7.5}, 10^{8.0} M_\odot$ at $z \sim 1, 2, 3$ while being complete for the oldest passive galaxies to $M_* \sim 10^{8.0}, 10^{8.5}, 10^{9.0} M_\odot$ at these redshifts (estimated following Pozzetti et al. 2010; Chartab et al. 2020). Our depth and area will enable an unprecedented study of dwarf galaxies and their environments.

Environmental effects are believed to be the primary reason of quenching in low-mass galaxies at $z < 1$ (e.g., Geha et al. 2012; Wetzel et al. 2013; Balogh et al. 2016; Fossati et al. 2017; Guo et al. 2017). However, the role of environmental quenching at higher redshift remains unclear due to scarce observations. Based on the predicted Roman $z_{\rm phot}$ accuracy (Khederlarian et al. 2026), our test shows that the 7^{th}-neighbor overdensity measured by RXDF at $1 < z < 3$ will recover local densities with a scatter of 0.25 dex. This is significantly smaller than the full dynamic range of environments (Poggianti et al. 2010), allowing us to statistically distinguish between voids, filaments, and clusters. At $1 < z < 3$, RXDF will robustly: (1) detect low-mass quiescent galaxies, (2) quantify

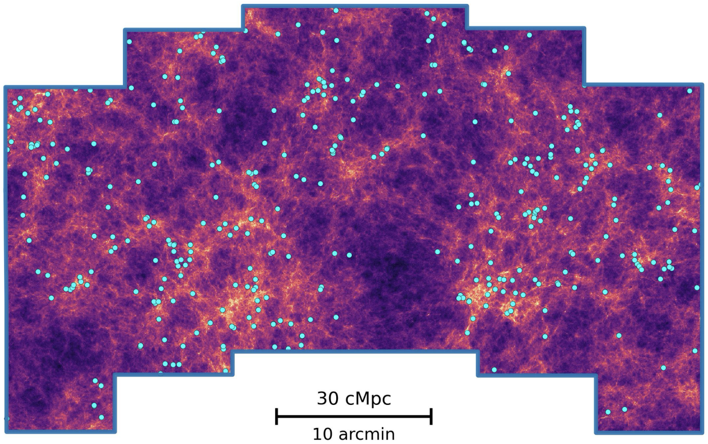

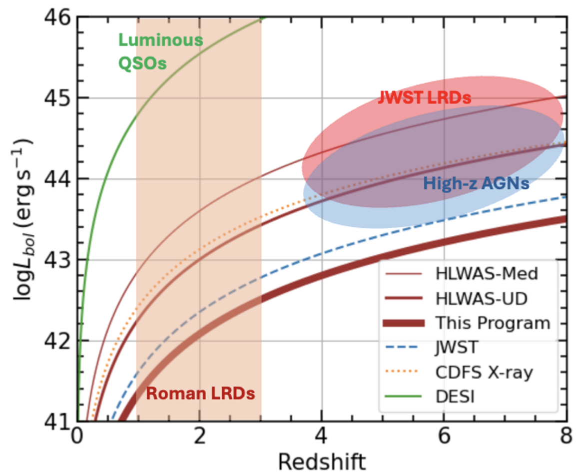

Figure 7. (**left**) Demonstration of early LSS from the TNG300 simulation following Wu et al. (2026). A slice at $z = 10$ with $\Delta z = 0.2$ (40 cMpc) is shown in the RXDF footprint. Galaxies of rest-frame $m_{\rm UV} < 30$ mag are indicated in cyan and show obvious LSS. Only RXDF can beat down the cosmic variance and properly interpret such early structures. (**right**) Bolometric luminosity and redshift space for AGNs and LRDs. RXDF will deliver the deepest AGN sample at $z \gtrsim 6$, on par with the deepest JWST AGN samples but with $\gtrsim$30–50$\times$ larger size. RXDF also probes cosmic-noon LRDs to $\sim$10$\times$ lower luminosity than high-z JWST LRDs.

quenching fractions across mass and environment, and (3) correlate galaxy morphology with local density. RXDF will provide the first comprehensive view of the multi-dimensional interplay between stellar mass, star formation, morphology, and environments in the dwarf regime at cosmic noon and afternoon and hence offer the most stringent constraints to date on early galaxy quenching.

4.2. *Accreting supermassive black holes (SMBHs)*

Identifying low-luminosity AGNs and measuring their physical properties towards cosmic dawn provide crucial insights on early SMBH growth and their coevolution with galaxies. AGN selection at the extreme faint-luminosity is challenging: contamination from host galaxy and photometric errors prevent robust AGN identification using traditional SED-based approaches (Lyu et al. 2024). RXDF will efficiently identify unobscured AGNs up to $z \gtrsim 6$ via sensitive variability detection over two years. AGNs vary more strongly in rest-frame UV than in longer wavelengths; our bands sample rest-frame UV at $z \gtrsim 6$ and therefore will be more sensitive than JWST in identifying early AGNs (Stone et al. 2025; Scholtz et al. 2025). The variability selection can also identify extremely faint AGNs at all redshifts, including dwarf AGNs ($\lesssim 10^{5-6}\,M_\odot$) at cosmic noon far beyond the reach of other programs. Our sample will probe $\sim$10$\times$ fainter than those from the HLWAS Ultra-Deep, reaching similar depths but considerably larger sample sizes compared with the deepest X-ray and JWST programs (Scholtz et al. 2025). This is illustrated in the right panel of Figure 7. Such a faint AGN sample would lead to a leap-forward in our understanding of SMBH formation, e.g., $L_{\rm bol} \approx 10^{42}\,{\rm erg\,s^{-1}}$ at $z \sim 2$ corresponds to a $10^4\,M_\odot$ (seed) black hole accreting at the Eddington limit.

RXDF will also enable crucial advances in studying Little Red Dots (LRDs), an enigmatic population discovered by JWST (Labbé et al. 2023; Kocevski et al. 2023; Harikane et al. 2023b; Matthee et al. 2024; Greene et al. 2024), with compact morphology, V-shaped SEDs, and abundant at high-z.

Their nature is debated, including dusty star formation, extreme accretion, and/or gas enshrouded accreting SMBHs (Akins et al. 2025; Inayoshi & Maiolino 2025; Lambrides et al. 2024; Naidu et al. 2025; Liu et al. 2025) that may hold the key to SMBH seed formation. Addressing this requires vastly expanding the samples at the faint end, uniquely achieved with RXDF pushing to luminosities $\sim$10$\times$ below the current JWST samples (with Roman LRDs at $z\sim1-3$) and >3 mag below the least luminous LRDs in the HLWAS Ultra-Deep. Our large area is necessary to yield the first statistically large samples at these uncharted low luminosities given their current estimated (albeit highly uncertain) space densities at Cosmic Noon (c.f. Ma et al. 2025). Moreover, their variability (Stone et al. 2025; Burke et al. 2025) will be probed to unparalleled depths. Our data will uniquely enable vast improvements in constraining and testing physical models of LRDs (Inayoshi & Maiolino 2025; Liu et al. 2025; Naidu et al. 2025; Secunda et al. 2026).

4.3. *High-z supernovae*

In our cadenced observations, each sub-epoch will reach AB = 28.8 mag in $RZYJH$, 27.8 mag in F and 26.8 mag in K, and each main epoch (stacks of 3 sub-epochs) will reach $RZYJH = 29.4$, $F = 28.4$ and $K = 27.4$ mag. These unprecedented sub-/single-epoch depths will probe uncharted parameter space for transient discovery, especially for high-**z** SNe. We will easily detect SNe at $z \geq 2.5$, complementing the HLTDS whose focus is SNe at $z < 2.5$. Our layered time cadences and multi-band light curves, aided by host galaxies' superb $z_{\rm phot}$, will allow SN classification with high confidence.

(1) *Thermonuclear SNe, or SNe Ia:* SNe Ia are currently the only standard candles extending the Hubble diagram to high-z and therefore are critical to precision cosmology. SNe Ia need white dwarf progenitors and cannot occur too early, however, it is believed that SNe Ia could begin at $z \sim 5$ (e.g., Riess & Livio 2006; Graur et al. 2011; Wiseman et al. 2021). With peak of $M \approx -19.3$ ($m = 27.1$ at $z = 5$), they can be easily detected *in a sub-epoch* (but missed by the HLTDS). We predict $\sim$200 SNe Ia *in each epoch*, of which $\sim$40 are at $z > 2.5$. The sub-epochs will well sample the light curves in the first 30 days of discovery to robustly select those near peak (expecting 6–22 of them) to enable cosmological applications.

(2) *Core-collapse SNe (CCSNe):* As the progenitors of CCSNe are high mass ($\gtrsim 8M_\odot$) stars, the rate of CCSNe constrains the high-mass end of their host galaxies' IMF, which is fundamental to understanding galaxy evolution. CCSNe can be detected out to $z \approx 8$ as transient Y-dropouts in our single-epoch images when near their peak ($M \approx -18.0$ mag, or $m \approx 29.2$ mag). We expect $\sim$400 CCSNe at $z > 2.5$ and $\sim$10 at $z > 6$.

(3) *Superluminous SNe (SLSNe):* With peak luminosity $M{<}{-21}$ mag, SLSNe can be detected out to $z \approx 14$ as transient F-dropouts (K=27 for M=−21 mag) in our single-epoch images. The 1-yr cadence corresponds to rest-frame $\sim$24 days at $z \approx 14$, which will provide sufficient time sampling. Based on the $z \sim$ 2–5 observations to date (Cooke et al. 2012; Prajs et al. 2017), RXDF will detect $\sim$80 SLSNe at $z > 2.5$. The progenitors of SLSNe must be very high-mass stars, and it is believed that pair instability could be a viable mechanism for SLSNe. Pop-III (i.e., metal-free) stars could end their lives as supernovae through pair instability, and therefore it is likely that the SLSNe found at the highest redshift from RXDF could contain Pop-III SNe.

4.4. *Broader science*

RXDF will enable a plethora of studies beyond the above, even extending to the studies of our Galaxy and the Solar System. Two examples are outlined below.

— Galactic cool dwarfs: Using colors, PSF shapes and proper motions, RXDF will identify and characterize the lowest-mass stars and brown dwarfs (BDs; $<0.1\ M_{\odot}$) through the thin and thick disks and deep into the halo. We will (a) measure thin disk scale height vs. temperature across the BD regime to examine evolutionary ages and mass-dependent scattering in the Galactic potential (Ryan et al. 2017; Aganze et al. 2022); (b) measure the LF and MF of the thick disk and halo across the star/BD limit for the first time; (c) build a large sample of halo BDs (>100) to explore abundance effects on low-temperature atmospheres (Burgasser et al. 2025) and thermal evolution across the star/BD gap; and (d) identify the lowest-mass stars of the outer halo (>100 kpc) and determine their kinematic alignment with stream populations.

— Moving objects in our Solar system: The Oort cloud comets (OCCs) have a significant chance of being near the ecliptic poles (Kaib & Quinn 2009), and each of our sub-epochs is ideal for their detection by shift-and-stack (e.g., Bernstein et al. 2004; Smotherman et al. 2021). At $R = 28.8$ mag for each sub-epoch, typical OCC objects (∼200 meters) are reachable at 4 AU. Towards larger distances, it has been posited that there should be substantial numbers of dynamically old comets beyond the orbit of Saturn (Kaib 2022), but these are too faint to be detected by any current surveys. RXDF's unprecedented area and depth will allow us to quantitatively test this hypothesis, placing stringent limits even in case of non-detection.

5. TENTATIVE DATA RELEASE PLAN

As per the general Roman data access policy, all the raw and Roman pipeline-processed data from our program will be immediately public. However, we anticipate carrying out some additional calibrations beyond the default pipeline, specific to the needs of our RXDF program, in order to optimize the data products for achieving the aforementioned science goals. We plan to release the team-vetted data products on an annual basis. To facilitate the science production by the community at large, we will also make best-effort, "quick releases" of our products described as follows.

◦ We plan to release the image products of each major epoch as soon as the validation is finished, which we expect will be one month after the completion of the observations for that major epoch. These include the images of each sub-epoch as well as the stacks of the three sub-epochs.

◦ The source catalogs will be released one month after the per-epoch image release.

◦ The search for transients will be carried out as soon as each sub-epoch is finished, and the results will be immediately announced through the TNS to facilitate possible follow-ups.

◦ The full-stacks of all data will be expected to be released one month after the last observation, and the accompanying source catalogs will also be released one month after the image release.

REFERENCES

Adams, N. J., Conselice, C. J., Austin, D., et al. 2024, ApJ, 965, 169, doi: 10.3847/1538-4357/ad2a7b

Aganze, C., Burgasser, A. J., Malkan, M., et al. 2022, ApJ, 934, 73, doi: 10.3847/1538-4357/ac7053

Akins, H. B., Casey, C. M., Lambrides, E., et al. 2025, ApJ, 991, 37, doi: 10.3847/1538-4357/ade984

Bagley, M., Finkelstein, S., Rhoads, J., et al. 2025, arXiv e-prints, arXiv:2603.09828, doi: 10.48550/arXiv.2603.09828

Balogh, M. L., McGee, S. L., Mok, A., et al. 2016, MNRAS, 456, 4364, doi: 10.1093/mnras/stv2949

Beckwith, S. V. W., Stiavelli, M., Koekemoer, A. M., et al. 2006, AJ, 132, 1729, doi: 10.1086/507302

Bernstein, G. M., Trilling, D. E., Allen, R. L., et al. 2004, AJ, 128, 1364, doi: 10.1086/422919

Bouwens, R. J., Illingworth, G. D., Oesch, P. A., et al. 2015, ApJ, 803, 34, doi: 10.1088/0004-637X/803/1/34

Bouwens, R. J., Oesch, P. A., Stefanon, M., et al. 2021, AJ, 162, 47, doi: 10.3847/1538-3881/abf83e

Bowler, R. A. A., Jarvis, M. J., Dunlop, J. S., et al. 2020, MNRAS, 493, 2059, doi: 10.1093/mnras/staa313

Bowler, R. A. A., Dunlop, J. S., McLure, R. J., et al. 2015, MNRAS, 452, 1817, doi: 10.1093/mnras/stv1403

Burgasser, A. J., Schneider, A. C., Meisner, A. M., et al. 2025, ApJ, 982, 79, doi: 10.3847/1538-4357/adb39f

Burke, C. J., Stone, Z., Shen, Y., & Jiang, Y.-F. 2025, arXiv e-prints, arXiv:2511.16082, doi: 10.48550/arXiv.2511.16082

Chartab, N., Mobasher, B., Darvish, B., et al. 2020, ApJ, 890, 7, doi: 10.3847/1538-4357/ab61fd

Cooke, J., Sullivan, M., Gal-Yam, A., et al. 2012, Nature, 491, 228, doi: 10.1038/nature11521

Dalmasso, N., Ferrami, G., Leethochawalit, N., Ventura, E. M., & Trenti, M. 2026, MNRAS, 546, stag001, doi: 10.1093/mnras/stag001

Donnan, C. T., McLeod, D. J., Dunlop, J. S., et al. 2023, MNRAS, 518, 6011, doi: 10.1093/mnras/stac3472

Donnan, C. T., McLure, R. J., Dunlop, J. S., et al. 2024, MNRAS, 533, 3222, doi: 10.1093/mnras/stae2037

Eisenstein, D. J., Johnson, B. D., Robertson, B., et al. 2025, ApJS, 281, 50, doi: 10.3847/1538-4365/ae1137

Eisenstein, D. J., Willott, C., Alberts, S., et al. 2026, ApJS, 283, 6, doi: 10.3847/1538-4365/ae3163

Ellis, R. S., McLure, R. J., Dunlop, J. S., et al. 2013, ApJL, 763, L7, doi: 10.1088/2041-8205/763/1/L7

Endsley, R., Behroozi, P., Stark, D. P., et al. 2020, MNRAS, 493, 1178, doi: 10.1093/mnras/staa324

Fossati, M., Wilman, D. J., Mendel, J. T., et al. 2017, ApJ, 835, 153, doi: 10.3847/1538-4357/835/2/153

Geha, M., Blanton, M. R., Yan, R., & Tinker, J. L. 2012, ApJ, 757, 85, doi: 10.1088/0004-637X/757/1/85

Graur, O., Poznanski, D., Maoz, D., et al. 2011, MNRAS, 417, 916, doi: 10.1111/j.1365-2966.2011.19287.x

Greene, J. E., Labbe, I., Goulding, A. D., et al. 2024, ApJ, 964, 39, doi: 10.3847/1538-4357/ad1e5f

Guo, Y., Bell, E. F., Lu, Y., et al. 2017, ApJL, 841, L22, doi: 10.3847/2041-8213/aa70e9

Harikane, Y., Ouchi, M., Oguri, M., et al. 2023a, ApJS, 265, 5, doi: 10.3847/1538-4365/acaaa9

Harikane, Y., Zhang, Y., Nakajima, K., et al. 2023b, ApJ, 959, 39, doi: 10.3847/1538-4357/ad029e

Illingworth, G. D., Magee, D., Oesch, P. A., et al. 2013, ApJS, 209, 6, doi: 10.1088/0067-0049/209/1/6

Inayoshi, K., & Maiolino, R. 2025, ApJL, 980, L27, doi: 10.3847/2041-8213/adaebd

Jespersen, C. K., Steinhardt, C. L., Somerville, R. S., & Lovell, C. C. 2025, ApJ, 982, 23, doi: 10.3847/1538-4357/adb422

Kaib, N. A. 2022, Science Advances, 8, eabm9130, doi: 10.1126/sciadv.abm9130

Kaib, N. A., & Quinn, T. 2009, Science, 325, 1234, doi: 10.1126/science.1172676

Khederlarian, A., Andrews, B. H., Newman, J. A., Zhang, T., & Dey, B. 2026, arXiv e-prints, arXiv:2602.10207, doi: 10.48550/arXiv.2602.10207
Kocevski, D. D., Onoue, M., Inayoshi, K., et al. 2023, ApJL, 954, L4, doi: 10.3847/2041-8213/ace5a0
Labbé, I., van Dokkum, P., Nelson, E., et al. 2023, Nature, 616, 266, doi: 10.1038/s41586-023-05786-2
Lambrides, E., Garofali, K., Larson, R., et al. 2024, arXiv e-prints, arXiv:2409.13047, doi: 10.48550/arXiv.2409.13047
Landy, S. D., & Szalay, A. S. 1993, ApJ, 412, 64, doi: 10.1086/172900
Lee, K.-S., Giavalisco, M., Conroy, C., et al. 2009, ApJ, 695, 368, doi: 10.1088/0004-637X/695/1/368
Liu, H., Jiang, Y.-F., Quataert, E., Greene, J. E., & Ma, Y. 2025, ApJ, 994, 113, doi: 10.3847/1538-4357/ae0c19
Lyu, J., Alberts, S., Rieke, G. H., et al. 2024, ApJ, 966, 229, doi: 10.3847/1538-4357/ad3643
Ma, Y., Greene, J. E., Setton, D. J., et al. 2025, arXiv e-prints, arXiv:2504.08032, doi: 10.48550/arXiv.2504.08032
Matthee, J., Naidu, R. P., Brammer, G., et al. 2024, ApJ, 963, 129, doi: 10.3847/1538-4357/ad2345
McLeod, D. J., Donnan, C. T., McLure, R. J., et al. 2024, MNRAS, 527, 5004, doi: 10.1093/mnras/stad3471
Muñoz, J. B., Mirocha, J., Furlanetto, S., & Sabti, N. 2023, MNRAS, 526, L47, doi: 10.1093/mnrasl/slad115
Muzzin, A., Marchesini, D., Stefanon, M., et al. 2013, ApJ, 777, 18, doi: 10.1088/0004-637X/777/1/18
Naidu, R. P., Matthee, J., Katz, H., et al. 2025, arXiv e-prints, arXiv:2503.16596, doi: 10.48550/arXiv.2503.16596
Naidu, R. P., Oesch, P. A., Brammer, G., et al. 2026, The Open Journal of Astrophysics, 9, 56033, doi: 10.33232/001c.156033
Oesch, P. A., Bouwens, R. J., Illingworth, G. D., Labbé, I., & Stefanon, M. 2018, ApJ, 855, 105, doi: 10.3847/1538-4357/aab03f
Oesch, P. A., Bouwens, R. J., Carollo, C. M., et al. 2010, ApJL, 709, L21, doi: 10.1088/2041-8205/709/1/L21
Paquereau, L., Laigle, C., McCracken, H. J., et al. 2025, A&A, 702, A163, doi: 10.1051/0004-6361/202553828
Poggianti, B. M., De Lucia, G., Varela, J., et al. 2010, MNRAS, 405, 995, doi: 10.1111/j.1365-2966.2010.16546.x
Pozzetti, L., Bolzonella, M., Zucca, E., et al. 2010, A&A, 523, A13, doi: 10.1051/0004-6361/200913020
Prajs, S., Sullivan, M., Smith, M., et al. 2017, MNRAS, 464, 3568, doi: 10.1093/mnras/stw1942
Riess, A. G., & Livio, M. 2006, ApJ, 648, 884, doi: 10.1086/504791
Ryan, Jr., R. E., Thorman, P. A., Schmidt, S. J., et al. 2017, ApJ, 847, 53, doi: 10.3847/1538-4357/aa85ea
Scholtz, J., Witten, C., Laporte, N., et al. 2024, A&A, 687, A283, doi: 10.1051/0004-6361/202347187
Scholtz, J., Maiolino, R., D'Eugenio, F., et al. 2025, A&A, 697, A175, doi: 10.1051/0004-6361/202348804
Secunda, A., Somerville, R. S., Jiang, Y.-F., et al. 2026, ApJ, 996, 6, doi: 10.3847/1538-4357/ae1f08
Shen, Y., Zhuang, M.-Y., Li, J., et al. 2024, arXiv e-prints, arXiv:2408.12713, doi: 10.48550/arXiv.2408.12713
Smotherman, H., Connolly, A. J., Kalmbach, J. B., et al. 2021, AJ, 162, 245, doi: 10.3847/1538-3881/ac22ff
Somerville, R. S., Yung, L. Y. A., Lancaster, L., et al. 2025, MNRAS, 544, 3774, doi: 10.1093/mnras/staf1824
Stone, Z., Shen, Y., Zhuang, M.-Y., et al. 2025, arXiv e-prints, arXiv:2509.19585, doi: 10.48550/arXiv.2509.19585
Sun, G., Muñoz, J. B., Mirocha, J., & Faucher-Giguère, C.-A. 2025, JCAP, 2025, 034, doi: 10.1088/1475-7516/2025/04/034
Tacchella, S., Eisenstein, D. J., Hainline, K., et al. 2023, ApJ, 952, 74, doi: 10.3847/1538-4357/acdbc6
Teplitz, H. I., Rafelski, M., Kurczynski, P., et al. 2013, AJ, 146, 159, doi: 10.1088/0004-6256/146/6/159
Wetzel, A. R., Tinker, J. L., Conroy, C., & van den Bosch, F. C. 2013, MNRAS, 432, 336, doi: 10.1093/mnras/stt469

Whitler, L., Stark, D. P., Topping, M. W., et al. 2025, ApJ, 992, 63, doi: 10.3847/1538-4357/adfddc

Willott, C. J., Desprez, G., Asada, Y., et al. 2024, ApJ, 966, 74, doi: 10.3847/1538-4357/ad35bc

Wiseman, P., Sullivan, M., Smith, M., et al. 2021, MNRAS, 506, 3330, doi: 10.1093/mnras/stab1943

Wu, Z., Eisenstein, D. J., Johnson, B. D., et al. 2026, arXiv e-prints, arXiv:2601.15960, doi: 10.48550/arXiv.2601.15960